 cmes, vol.5, no.6, pp.527-539, 2004

Atomistic Simulations of Dislocation-Void Interactions using Green's Function Boundary Relaxation

Xiangli Liu[1], S. I. Golubov[1], C. H. Woo[1,2] and Hanchen Huang[3]

Abstract: A Green's function technique is developed for the relaxation of simulation cell boundaries in the modelling of dislocation interactions using molecular dynamics. This method allows the replacement of fixed or periodical boundary conditions with flexible boundary conditions, thus minimizing the artificial effects due to images forces introduced by the fixed boundary condition, or the periodic repetition of simulation cells. The effectiveness of the Green's function in the removal of the fixed boundary image forces is first checked in the atomistic simulation involving the glide of the $a/2<110>$ dislocation in bcc tungsten. This method is then applied to study the reaction of an edge dislocation with voids in tungsten. The simulation results are compared with predictions from the continuum model.

keyword: Crystal, Green's function, atomistic simulations, dislocation dynamics

1 Introduction

Computer modeling has been widely used to study crystal properties, particularly those of the crystal defects, such as the core structure and energetics of dislocations, and their role in the mechanical properties of crystals (Ghoniem and Cho, 2002, Srivastava and Atluri, 2002). Thus, calculations of the Peierls stress of dislocations, their mobility, and their interactions with various other crystal defects, are of special interest in understanding the plasticity of materials through the dynamics of dislocation. Some of the pioneering work in this area involves the calculation of the lattice friction stress in the late sixties and seventies [Gehlen, Rosenfield and Hahn (1968); Granzer, Wagner and Eisenblatter (1968); Basinski, Duesbery and Taylor (1972); Hoagland, Hirth and Gehlen (1976); Woo and Puls (1976); Puls and Norgett (1976)]. These calculations are mostly for infinite straight dislocations, due to the restriction imposed by the treatment of the simulation cell boundaries available at that time. Three types of boundary conditions are generally used. The rigid (fixed) boundary [Gehlen *et.al*., (1968); Granzer *et.al* (1968); Basinski *et.al.* (1972); Puls and Norgett (1976)], the periodic boundary [Daw, Baskes and Wolfer (1986); Moncevicz, Clapp and Rifkin (1990); Daw, Foiles and Baskes (1993); Chang, Bulatov and Yip (1999); Rodney and Martin (1999); Rodney and Martin (2000); Diaz de la Rubia, Zbib, Khraishi, Wirth, Victoria and Caturia (2000)], and the flexible boundary employing the line Green function [Hoagland *et.al* (1976); Woo and Puls (1976)]. More recently, the Molecular Dynamics (MD) technique is used to study the mobility of non-straight dislocations, such as jogged $a/2<110>$ edge dislocation and their interactions with interstitial clusters in fcc Ni [Rodney and Martin (1999, 2000)], and $a/2<110>$ edge dislocation interacting with stacking fault tetrahedra in fcc Cu [Diaz de la Rubia, Zbib, Khraishi, Wirth, Victoria and Caturia (2000)]. Liu, Shi, Woo and Huang (2002) studied the nucleation of dislocations in thin films. In these calculations, basically, the periodic boundaries, or a mixture of periodic and fixed boundaries are assumed.

It is well known that the results of the MD simulation of a moving dislocation in a finite computational cell are strongly affected by the conditions assumed at the cell boundaries (see Olmsted, Hardikar and Phillips (2001); Ohsawa and Kuramoto (1999) for overviews). Assuming periodicity in all three orthogonal directions is the simplest methodology. However, since this boundary condition is not consistent with the existence of a net Burgers vector in a simulation cell, only dislocation dipoles or quadruples can be treated this way with any rigor. Otherwise, images forces produced by the periodic repetition of simulation cells, may produce unrealistic results. Another method assumes periodicity in two directions only

[1] Department of Mechanical Engineering, The Hong Kong Polytechnic University, Hong Kong

[2] Communicating author: Fax:+852-2365-4703, E-mail: chung.woo@polyu.edu.hk

[3] Department of Mechanical, Aerospace & Nuclear Engineering, Rensselaer Polytechnic Institute, Troy, NY 12180

(in the glide direction and the line direction), but fixed boundaries (or partially fixed) on each side in the third direction. Such a method allows the simulation of a single dislocation in the computation cell, but the forces between the dislocation and its images across the fixed boundaries may considerably distort the dislocation core, and directly affect its motion. This also happens similarly to the case where pure periodic boundary conditions are applied.

It is worthwhile noting that the results obtained this way are, rigorously speaking, only relevant to a system of dislocations situated periodically at a fixed distance along the direction of the Burger's vector. Thus, one has to be careful when comparing the simulation results with those from macro-models based on the "single dislocation in an infinite medium" approach. Moreover, these methods are not suitable for application to dislocations with a screw component. A satisfactory method for the simulation of 3D dislocation dynamics, for dislocations of both the screw and edge type, is very much in need. This is the subject of investigation of the present paper.

Several attempts to solve the image-force problem have been made via the so-called flexible boundary method, the earliest works of which has been reviewed by Vitek (1974) and Perrin (1974). Subsequently, making use of the periodicity along the dislocation line in a scheme called Flex-II, Hoagland *et.al.* (1976) apply the line-force Green's function (GF) of Hirth, and Lothe (1973) to re-arrange the atoms after relaxation of the primary atomistic region (Region I) to achieve relaxation of the boundary forces. The effectiveness of this scheme suffers because the elastic GF diverges when the field point, at which the displacement is evaluated, is close to the source point. In a separate attempt, Sinclair, Gehlen, Hoagland and Hirth (1978) achieve relaxation of the boundary region by solving the anisotropic linear elastic problem outside the atomistic region to high order terms (Flex-HT). Woo and Puls (1976, 1977) modify the Flex-II scheme to calculate the Peierl's barrier, configuration and energy of an $a/2<l10>$ edge dislocations in MgO, by employing a "lattice" GF for very close separations between the source and field points. Iterative alternate applications of the atomistic and GF relaxations reduce the forces below tolerance quickly and effectively in all regions. This turns out to be the most efficient scheme for single dislocations, according to Sinclair *et.al.* (1978) and Puls and Woo (1975).

The 3D GF boundary relaxation method (GFBR) recently proposed by Rao, Hernandez, Simmons, Parthasarathy and Woodward (1998), further extends the earlier flexible boundary methods to applications beyond the single straight dislocation. Instead of using the GF for infinite lines of atoms in the earlier flexible boundary methods, the GFBR method calculates the relaxation of body forces acting on individual atoms, using the 3D-GF. The GFBR method has been introduced for the study of static dislocation properties only. Despite the successful application of the line-force GF to problems involving moving dislocations by Woo and Puls (1976), the extension of GFBR to studies involving moving dislocations has yet to be considered.

The GFBR method employs an iterative procedure, in which complete relaxation in the atomistic region is followed by GF relaxation of the cell boundaries and continuum regions. Under static conditions, the iterative process results in a minimum-energy, zero force, configuration of the system of atoms. Under dynamic conditions, however, it is more complex because in general a minimum-energy configuration does not necessarily exist. Yet, in this case, with each relaxation in the atomistic region, which is essentially a MD calculation in a crystal with fixed-boundaries, a quasi-minimum-energy configuration can be reached due to the development of the image forces. It is then unclear whether the GFBR technique is capable of relaxing the lattice configuration of the cell boundaries, to sufficiently reduce the build up of image forces that may disturb the iteration process. In this regard, it has been shown by Liu, Golubov, Huang and Woo (2003) that a single application of the 3D-GF may produce an energy reduction of about 80% through the relaxation. Under such a deep level of relaxation provided by the GF application, it is hopeful that a large build-up of image forces, sufficient to seriously interfere with the iteration process, can be avoided. We will test the method in this regard, in some detail, through an atomistic simulation study of the mobility of an edge $a/2<111>(110)$ dislocation under the action of a pure shear stress.

The present paper is organized as follows. Sec. 2 describes the method and the computational details. The simulation results for a moving dislocation are presented and analyzed in Sec.3. In Sec. 4, the application of the present method to the interaction of an edge dislocation with a void is presented and the results compared with

the continuum model. A short summary is given in Sec. 5.

2 Methodology and computational details

The 3D GFBR method used in the present calculation is essentially similar to the earlier modified Flex-II method, a comprehensive description of which has already been given by Rao *et. al.* (1998), and will not be repeated here. In general, the flexible boundary condition can be mixed with other types of boundary conditions, periodic or fixed. Simulation cells, in which all boundaries are flexible, have been used in static simulations (see e.g. [Rao *et.al.* (1998)]). However, this is not suitable for studies involving moving dislocations, because, due to the static nature of our 3D GF, the GFBR method cannot describe the time-dependent field of a moving dislocation. Furthermore, displacements of atoms near the dislocation core may be more than 10% of the lattice parameter, while for atoms in a perfect crystal environment, the displacements caused by stresses of a similar magnitude, being linear elastic in origin, are one- to two- orders of magnitude smaller. Even in the static simulations of a dislocation with an isolated kink in an unstressed crystal [Rao *et.al.* (1998)], it has already been noted that, "some of the forces that develop as the dislocation threads through the GF region at the end of the 3D cell cannot be optimized". This result reflects the different characteristics of atoms near the dislocation core compared to those in the perfect crystal, in their response to body forces. Although this effect may not be significant in static simulations, the situation may be much more serious under dynamic conditions, since "unrelaxed" forces may accumulate in the boundary region and eventually lead to the complete failure of the simulation.

Thus, the 3D GF technique can be used for simulation studies involving moving dislocations, only if the dislocation does not thread through the GF region. This condition may be satisfied by using periodic boundary conditions in the direction along the dislocation line. In the present paper this type of simulation cell is used.

The calculation in the present paper follows a procedure similar to that used in static calculations. After each complete MD relaxation in the atomistic region, a GF relaxation in all regions (atomistic, GF and continuum) is performed. The MD relaxation process in the atomistic region is achieved as usual by moving atoms according to Newton's equations of motion, and setting velocity components of those atoms to zero for each time step, if its sign is opposite to the corresponding force component acting on the atom. The Newton's equations of motion are integrated, with respect to time, with a time step of $\Delta t = 10^{-14}$ sec. Relaxation of the atomic configuration in the MD region causes forces on atoms in the GF and continuum regions, which are fixed during the MD calculation. We note that it is the action of these forces that collectively produce the image forces on the dislocation in the MD region.

During the subsequent GF relaxation, forces on each atom in the GF region are relaxed by displacing all atoms around it in the entire crystal according to the 3D GF, which has been modified to take into account periodic boundary condition along the dislocation line. In this calculation, we use GFCUHEX [Golubov, Liu, Huang and Woo (2001)], which has been written to calculate the displacements according to the elastic GF in cubic and hexagonal crystals. An advantage of GFCUHEX lies in the use of a matrix method that improves the computation efficiency by two orders of magnitude, compared to conventional methods based on the integral calculations. Indeed, this is a major factor that makes the present 3D flexible boundary method feasible at all.

The lattice GFs for the region close to the source of the point force, where linear elasticity fails, is calculated using the method described in Rao *et.al.* (1998). Displacements due to the lattice and elastic GFs agree with each other beyond a certain distance between the "source and field atoms". This is illustrated in Fig.1 where the ratio of the G_{11} components of the lattice and elastic GFs are calculated for the first nine shells is plotted. Similar behavior was also observed for other components of the GFs. This comparison shows that atoms are displaced according to the elastic GF, if its distance from the source of the point force is larger than $2.5a$, a being the lattice parameter, i.e. within the first nine shells. The lattice GF is used for smaller distance.

3 Quasi-dynamic simulation of a moving dislocation

To ensure that the accumulation of body forces in the boundary regions will not produce image forces on defects and their structures, which may excessively interfere with the evolution of the defect in the present scheme, the development of such forces during the motion of an $(a/2)[111](10\overline{1})$ edge dislocation under an applied shear, is monitored. The many-body potential for

tungsten [Ackland and Thetford (1987)] is used. An ideal bcc lattice with a lattice constant of 0.31652nm is first constructed with the lattice vectors [111] (*x*-direction), $[1\bar{2}1]$ (*y*-direction) and $[10\bar{1}]$ (*z*-direction). The computation cell is in the form of a cylinder with the cylindrical axis measured 12.4 nm in the *y*-direction (about $45b$), where b is length of the Burgers vector ($b = (\sqrt{3}/2)a$ =0.27411nm). Periodic boundary condition is assumed along the dislocation line in the *y*-direction. The cylindrical computation cell is elliptical in the $x-z$ plane, being elongated in the *x*-direction [111], i.e., the slip direction. The elliptical semi-axes are 7.22 nm (about $26b$) along the *x*-direction and 4.75 nm (about $17b$) along the *z*-direction. The lengths of the semi-axes in MD region along the $x-$ and $z-$ directions are 6.05 nm (about $22b$) and 2.99 nm about $11b$), respectively. The total number of atoms in the MD region is 44631.

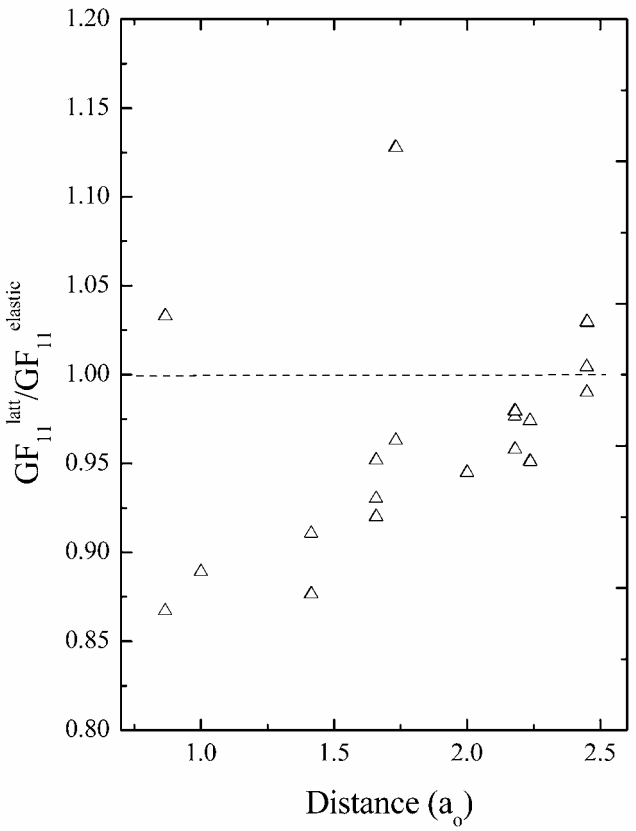

Figure 1 : Ratio of the lattice and elastic point force GF components, G_{11}, for the first nine coordinate shells in bcc tungsten as a function of distance R.

The $(a/2)[111](10\bar{1})$dislocation in the atomistic region is introduced at the center of the simulation cell, with the line along cylindrical axis, i.e., the *y*-direction, by displacing all atoms according to the isotropic linear elasticity theory, and then relaxing the system with the method described. The number of units for proper relaxation of the boundary forces is found to be seven (k = 3 in the Eq. 14 of Rao *et.al*. (1998)]). A homogeneous pure shear stress, σ_{zx}, in the $x-$direction on the $x-y$ plane, is applied by displacing atoms in all regions according to the corresponding homogeneous linear elastic strain. The calculations are performed with applied stresses in the range between 0.4 and 1.0 GPa, corresponding to 0.25% to 0.625 % of the shear modulus, μ.

Since our dislocation is moving very slowly, the configuration of the dislocation during the glide process can be clearly recognized, its glide plane being a known constant in the calculation. Indeed, the "extra half plane" for the edge dislocation in a bcc crystal consists of three (111) planes. Atoms that belong to these planes near the slip plane, can be easily identified on the $\{1\bar{2}1\}$plane (i.e., $x-z-$plane), from which the location of the dislocation core along the dislocation line can be obtained. Noting that the "extra plane" consists of three (111) planes and the slip plane consists of two $(10\bar{1})$ planes, the core of the dislocation has a width of b in $<111>$ (*x*-direction) and $\sqrt{2/3}b$ in $<10\bar{1}>$ (*z*-direction). This method is simple and straightforward, and is consistent with the centro-symmetric parameter method, and the disregistry method.

To monitor the accumulation of sources forces on atoms in the boundary region as the relaxation takes place in the MD region, we define the quantity $<F_{GF}>$:

$$< F_{GF} >= \sqrt{\frac{1}{N_{GF}} \sum_{i=1}^{N_{GF}} \left(F_{ix}^2 + F_{iy}^2 + F_{iz}^2 \right)}, \qquad (1)$$

where F_{ix}, F_{iy},F_{iz} are the Cartesian components of the force acting on the atom i, and N_{GF} is the total number of atoms in the GF region. We note that $<F_{GF}>$ so defined in equation (1) neglects the contributions from the small forces in the continuum region. Nevertheless, we anticipate $<F_{GF}>$ to give a good measure of the image forces on the dislocation.

The dislocation is allowed to relax in the absence of an applied stress for 0.16 ns, during which the GF relaxation

is repeated at 0.02 ns intervals. After that, a pure glide shear stress is applied, at about ten times the magnitude of the Peierls stress [Liu *et.al.* (2003)]. The simulation was carried on for about 0.5 ns, with the GF relaxation applied at 0.05 ns intervals.

The dislocation position, $<F_{GF}>$, and energy change as functions of time are shown in Fig. 2a-2c, respectively. The dotted line marks the application of the applied shear. In addition, $<F_{GF}>$ is also plotted in Fig.2d, as a function of the displacement of the dislocation. In Figs. 2a and 2c it can be seen that both $<F_{GF}>$ and the energy of the system tends to saturate during the relaxation in the unstressed crystal. Note that the value of $<F_{GF}>$ at equilibrium is non-zero (about 3×10^{-2} eV/nm), but is just sufficiently small to have negligible effects on the stability and the final atomistic configuration of the dislocation.

In Fig. 2a, $<F_{GF}>$ increases significantly when the applied stress is turned on and the dislocation starts to glide away from the starting position during the relaxation of the atomistic region (see Fig. 2b). In Fig. 2d, it is clear that $<F_{GF}>$ increases linearly with the displacement x. At the end of each relaxation cycle of the atomistic region, the dislocation slows down and the magnitude of $<F_{GF}>$ tends to saturate. The saturation occurs in response to the image-forces buildup under the fixed boundary conditions, which acts to oppose further advance of the dislocation under the applied shear [Woo and Puls (1976); Hull and Bacon (2001)]. Thus, in the present case, the total image force opposing the dislocation motion mainly comes from the two (111) fixed boundaries. For an edge dislocation at a distance x from the mid-point between fixed boundaries separated at a distance of $2b$ apart, the image force on the dislocation F_{im} can be easily calculated [Hull and Bacon (2001)] and put in the form $F_{im} = -Ax$, where

$$A = \frac{\mu}{2\pi(1-\nu)}\left(\frac{b}{d}\right)^2\left(1-\frac{x^2}{d^2}\right)^{-1},$$

is a weak function of x, for $x < d/2$. F_{im} increases approximately linearly with x as the dislocation moves towards the cell boundary. For a separation of $40b$, A has a value of $\sim 0.7\times10^{-3}\mu$ eV/b^3, and at a distance of less than $8b$, this image force would already be sufficiently large to completely cancel a sizable applied shear of up to $10^{-2}\mu$ on the dislocation. This slowing down of the dislocation motion during each fixed boundary relaxation cycle is indeed reflected in the displacement-time curve of the dislocation in Fig.2b.

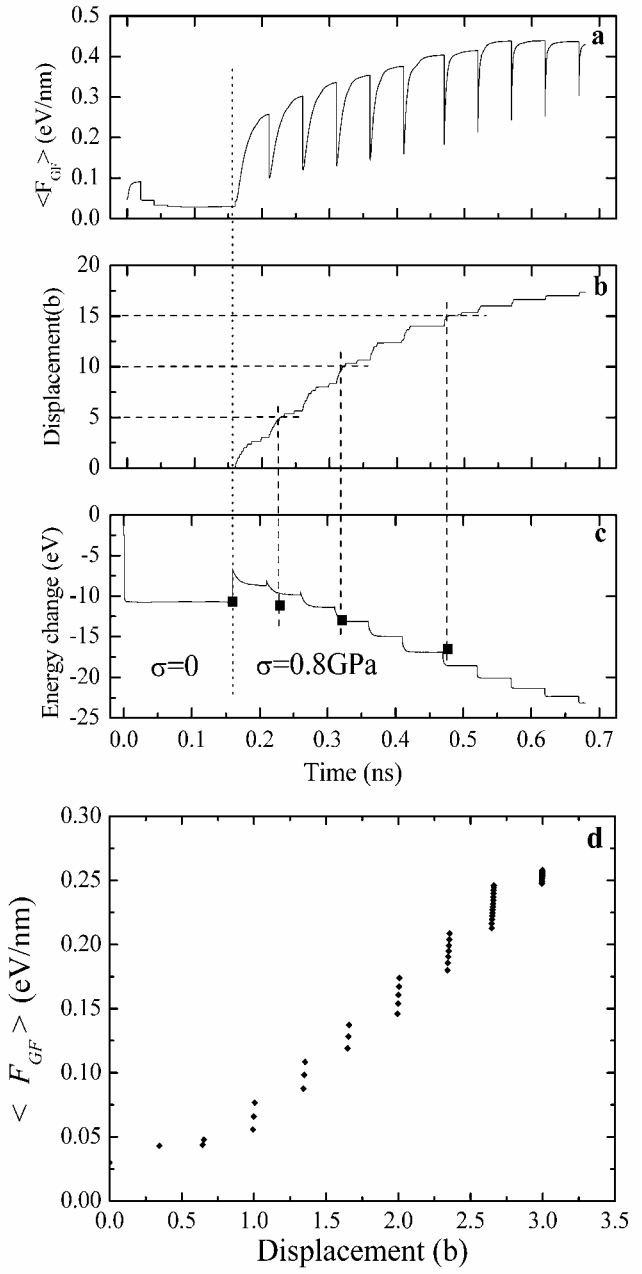

Figure 2 : (a) Time dependence of the mean force in GF region, $<F_{GF}>$, (b) displacement of the dislocation, (c) energy change of the crystal, unstressed, and during glide of the dislocation and (d) displacement vs $<F_{GF}>$ under pure shear stress 0.005μ, relation between $<F_{GF}>$ and displacement.

Comparison with Fig. 2d reveals that $F_{im}$is directly proportional to $<F_{GF}>$, the magnitude of which then re-

flects the magnitude of F_{im} ($F_{im} \sim 0.8 < F_{GF} >$). Each application of the GF reduces $< F_{GF} >$ and the image force against dislocation motion, thus rejuvenating the dislocation glide and allowing dislocation motion to continue during the entire simulation process.

The foregoing calculation shows that boundary relaxation achieved by the application of the GF is very effective in reducing the image force opposing the dislocation motion in its attempt to attain a lower energy configuration. This is particularly true when the dislocation is near the center of the simulation cell. In Fig. 2a the GF relaxation, though effective, does not completely reduce the mean force in the GF region to zero. In this regard, we note that with each GF application, not only the positions of the atoms in the GF region are adjusted, those in the atomistic region are also adjusted. The errors involved in the use of the perfect crystal GF in the defected atomistic region, and the use of the lattice GF are the main causes for the incomplete relaxation.

We note that the low force level before the application of the shear at 0.15 ns corresponds to a static situation, in which the applied stress is absent and the dislocation is not moving. After 0.15 ns, the GF is applied to a dynamic situation in which the applied shear is maintained, and the dislocation is moving. Indeed, the increase in the strain energies of the crystallite due to the application of the shear is obvious in Fig. 2c, at 0.15 ns. It is reasonable to speculate that the resulting contribution of this increase may explain the higher residual boundary forces after the subsequent GF relaxations.

The time dependence of the energy stored in the simulation cell provides another measure of the effectiveness of the GF boundary relaxation scheme presented here. It can be seen from the Fig. 2c that the total energy of the crystallite decreases when the dislocation move through the crystal. Such a decrease is related to the strain energy stored in a crystal of finite size with a dislocation moving under an applied shear. The filled squares plotted in Fig. 2c correspond to the difference in energy of the unstressed crystal containing the dislocation located at x= 0, 5, 10 and 15b with respect to that of the dislocation located at x= 0. It can be seen from this plot that the energy changes under dynamic and static conditions follow each other quite well.

We note that our calculation is only quasi-dynamic, and the speed of the dislocation is only apparent. The effect of the image forces must be taken into account if one is interested in the true dynamical behavior.

4 Dislocation-void interaction

The interaction of a dislocation with an obstacle in a form of a void can be considered within the continuum model of dispersion-strengthening, developed by Russell and Brown (1972) (R&B), for second-phase particles with a shear modulus lower than that of the matrix. In this connection, an obstacle in the form of voids is a limiting case in which the second-phase particles have zero shear modulus. Thus in accordance with the R&B model, the yield stress τ due to voids placed on the slip plane at a distance L apart is given by

$$\tau = \frac{\mu b}{L} \begin{cases} 0.8 \left[1 - \left(\frac{\ln(R/r)}{\ln(R/r_c)} \right)^2 \right]^{1/2}, & \phi \leq 100^o, \\ \left[1 - \left(\frac{\ln(R/r)}{\ln(R/r_c)} \right)^2 \right]^{3/4}, & \phi \geq 100^o, \end{cases} \tag{2}$$

where ϕ is the critical angle at which the dislocation cuts a void of the radius r. In Eq. 2, μ is the shear modulus, b is the Burgers vector and R, r_c are the cut-off radius and the core radius of the dislocation, respectively. Note that $\tau = 0$ when $r \leq r_c$.

As can be seen from Eq. 2 the yield stress τ at a given void spacing, L, is a function of the void radius, r, critical angle, ϕ, and dislocation core radius, r_c. The core radius can be calculated by the standard method (see e.g. [Xu and Moriarty (1996)]). It is one of our aims, in this paper, to investigate the limitations of the continuum R&B model by comparing with the results of computer simulation, in terms of the yield stress τ and critical angle ϕ as a function of void size.

An $(a/2)[111](10\bar{1})$ edge dislocation is introduced into the simulation cell with the center at $x = -8b$ and z= 0 by the method described in the section 2. The asymmetrical position along the slip direction is chosen to keep the dislocation near the center of the atomistic region during the course of the calculation. The initial configuration is relaxed for 0.09 ns, with a GF relaxation applied after 0.05 ns. After that a void is introduced into the crystallite by removing a set of atoms with the coordinates located in a sphere centered on the dislocation line in the middle of the simulation cell in $y-$ direction. The atomic configuration of the dislocation and the void was further relaxed in an unstressed crystal for 0.08 ns with two GF relaxations after each 0.03 ns.

We note that, to save computation time without losing the essential physics of the process, the void is directly placed with its center on the dislocation line, a position corresponding to an energy minimum. Indeed, due to the reduction of the dislocation line length, the process involved when an edge dislocation enters into a void is energetically favorable. As a result, the energy of a crystal minimizes when a void is placed with its center at the dislocation line, and such a configuration will be arrived at, regardless of the initial distance between the moving dislocation and void. When the dislocation line moves away from the void center to void surface and starts to lengthen, the energy increase is the cause of the strengthening.

A constant pure shear stress in the $x-$direction on the $x-y$ plane is then applied. After that the atoms are allowed to relax as described in the foregoing for a time period of $\sim$1ns, with GF relaxations applied at 0.05 ns intervals. Similar to the case in subsection 2, the mean force $<F_{GF}>$ and the total energy of the system are monitored during the calculation. In addition, the configuration of the dislocation line and the mean dislocation displacement in the glide direction, are also recorded. The calculation is repeated, with applied stresses increased at a step size of $\Delta\sigma$ = 0.1 GPa, to determine the minimum stress, i.e., the yield stress, τ, needed for the dislocation to break away from the void. The calculations have been performed for voids with three different sizes.

The time dependence of the mean force $<F_{GF}>$, mean dislocation displacement, and energy change, are presented in Fig. 3. The dash and solid lines correspond to shear stresses of 0.6 and 0.7 GPa, respectively. To facilitate description, the plot is divided into four time periods marked by numbers from I to IV.

During period I, the crystallite containing the dislocation and void is relaxed in the absence of the applied shear. Both the mean force $<F_{GF}>$ and the energy converge at the end of this period. Note the time dependence of the energy change in this period is not shown in Fig. 3c, because the relaxation takes place without the void and is similar to that presented in Fig. 2c.

Period II in Fig. 3 corresponds to the initial dislocation movement when the applied shear is applied. It can be seen from Fig. 3a that in this time period, the mean force $<F_{GF}>$ gradually decreases with time for both low and high stresses. Moreover each GF relaxation decreases $<F_{GF}>$ to a level, which is only slightly higher than that in the unstressed crystal. Such a behavior is different when the void is absent (see Fig. 2). In this case the magnitude of $<F_{GF}>$ is larger and on the average increases with time. This difference may be understood, because in the presence of a void, the total resistance to the movement of the dislocation is higher than in its absence where the resistance is due to the fixed boundary conditions only.

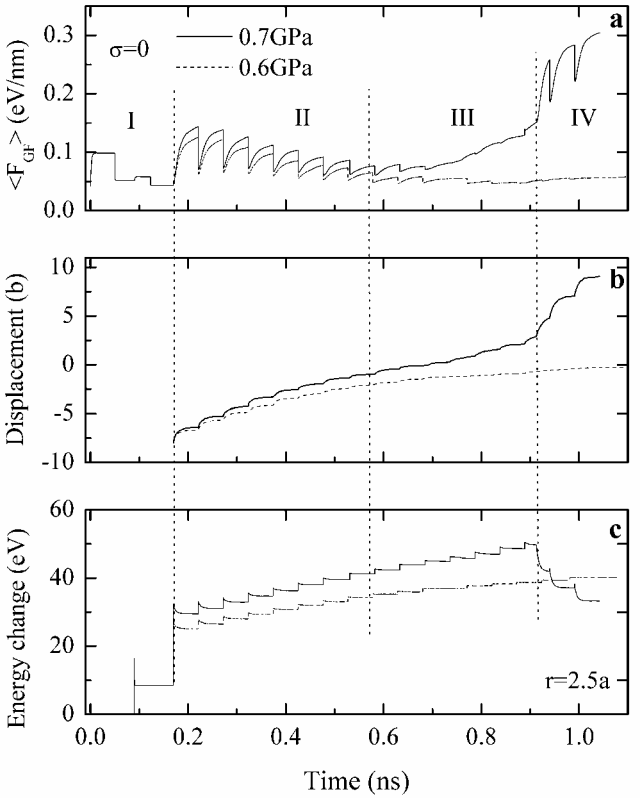

Figure 3 : Time dependence for the same values as in Fig.2 for the case of interaction the dislocation with VOID-II under pure shear stress σ_{xz} = 0.7 GPa (solid line) and 0.6 GPa (dashed line). The dotted lines mark the times corresponding to introduction of the dislocation and void, loading the shear stress and dislocation braking free of the void, respectively. Note that the energy of the system increases during the dislocation-void interaction therewith the effect takes place as a result of GF relaxation.

In the presence of the void, the dislocation displacement during each relaxation in the atomistic region is smaller, resulting in a reduced $<F_{GF}>$. Consequently, each GF application leads to a deeper relaxation. In both cases of low and high stresses the dislocation moves through

the void although the effective speed of the dislocation is slightly different (see Fig. 3b).

In period III, the evolution of $<F_{GF}>$ is primarily different for the two different stresses. At the low stress, the mean force $<F_{GF}>$ has a clear tendency to saturate at a low level, close to that in the unstressed crystal. This process continues in period IV, where the mean displacement and energy become constant. This behavior shows that the dislocation is trapped by the void, i.e. the applied stress is below the yield stress.

With the higher applied stress of 0.7 GPa, the mean force $<F_{GF}>$ increases with time in Period III, and its reduction due to the GF relaxation becomes very small. At the same time the dislocation is moving slower less than in period II (see Fig. 4). It shows that in this period the dislocation movement is mainly controlled by its interaction with the void. At the end of the period, the effective glide speed starts to increase, and finally the dislocation breaks away from the void. Thus the yield stress is determined to be between 0.6 and 0.7 GPa, and we take it to be 0.7 GPa.

Note that for the higher stress case, in period IV the dislocation moves through the perfect crystal with a speed close to that at the beginning of the period II, i.e. when the dislocation just starts to move. Moreover the $<F_{GF}>$ dislocation displacement and energy change in period IV depend on time in a way similar to that in Fig. 2.

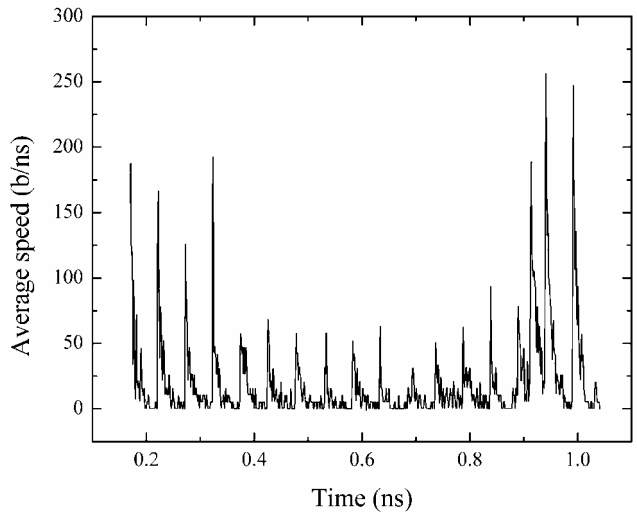

Figure 4 : The effective speed of the dislocation during it interaction with the VOID-II under critical stress of σ_{xz} = 0.7 GPa. Note that the speed is about the same at the beginning and end of dislocation movement.

The time dependence of the energy in Fig.3c is of particular interest. Indeed, there is an overall increase of energy with time, when the dislocation is pinned by the void (e.g. in periods II and III in the case of the higher stress). However this increase occurs only with the GF relaxation. The energy actually decreases between the GF applications during relaxations in the atomistic region. Such a difference in the energy behavior caused by the atomistic and GF relaxations reflects an essential difference in their nature. Thus the former operates in the atomistic region only, i.e. in the closed system of atoms (atoms in the atomistic region together with ones in GF and continuum regions). In this case the energy unavoidably decreases during the relaxation. In contrast, the GF relaxation operates in the entire crystal, and represents the response of the "infinite crystal" on the atomic configuration change in the atomistic region. In this case, the computational cell is only a part of the infinite crystal, and the atoms in the simulation cell do not form a closed system.

Consequently the total decrease in energy of the infinite crystal, caused by the dislocation moving through the crystal, does not necessarily lead to an energy decrease in a sub-system. This is the case when the void-pinned dislocation bows out under an applied stress.

There are two reasons for the energy increase during the dislocation bow-out process. First, the length of the dislocation increases when the dislocation bows out. Second, it is related to the geometry of the calculations, namely during the dislocation bow-out process the dislocation moves towards the center of the simulation cell (see Fig. 5) where the strain energy of the dislocation stored in the finite crystal takes a maximum value (see previous paragraph). Actually in the time period IV, i.e. after the dislocation breaks away from the void, the energy rapidly decreases due to the same reason, when the shape of the dislocation returns to a straight line (see Fig. 5b) and as it moves away from the center of the simulation cell (see Fig. 5b).

We wish to emphasize that such energy behavior cannot be obtained with other methods, for example, when the two- dimensional periodic boundary conditions are used [Rodney and Martin (1999); Rodney and Martin (2000); Diaz de la Rubia, Zbib, Khraishi, Wirth, Victoria and Caturia (2000)]. Indeed, such simulation methods are based on the atomistic relaxation of a close system of atoms when any calculation in unstressed or stressed crystals

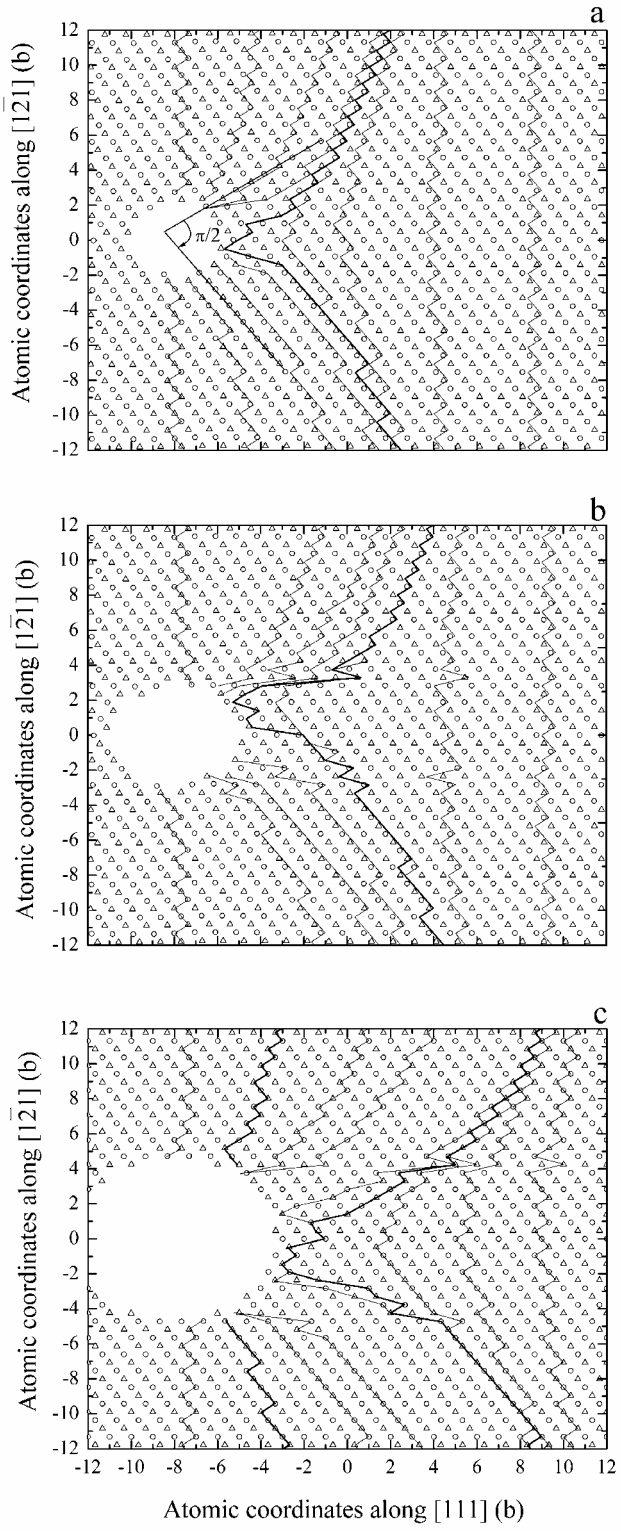

Figure 5 : Snapshots of the edge dislocation projected on the $(10\bar{1})$ plane in a process of interaction with voids of different sizes. Snapshots presented in the plot (a) to (c) correspond the cases of VOID-I, VOID-II, and VOID-III, respectively. Circles and triangles correspond the projection of the atoms located to two $(10\bar{1})$planes.

will always result in an energy decrease regardless of the process simulated. This difference in energy behavior between the present results and those obtained using other methods is related to the difference in the dislocation dynamics of a single dislocation and an array of dislocations.

The simulation results for the time evolution of the mean force $<F_{GF}>$, dislocation displacement and energy change obtained for VOID_I and VOID_III are qualitatively similar to that in Fig. 4. It is found that the yield stress is equal to 0.5 and 1.0 GPa in the case of VOID-I and VOID-III, respectively. Thus, one may infer that the yield stress increases with increase of the void size, which agrees qualitatively with the predictions of the R&B model. However, a quantitative comparison requires an estimate of the critical angle, ϕ, for the voids and the core radius r_c.

We next estimate the critical angle, ϕ. In Fig. 5a-5c, snapshots of the dislocation configurations projected on the$(10\bar{1})$ plane for voids of different sizes under the critical stresses of 0.5, 0.7 and 1.0 GPa are presented. The circles and triangles show the positions of atoms belonging to the two $(10\bar{1})$ glide planes (see Section 2) projected on the $(10\bar{1})$ plane in the unstressed crystal.

As can be seen from Fig. 6 the dislocation configurations prefer to be lined in parallel to the crystallographic directions in $<111>$ plane, in all cases. Consequently, arms of the dislocation when it is about to break away from the void (those configuration drawn by the thick lines) are not symmetrical with respect to the [111] direction. The critical angle, ϕ (i.e. the angle between the arms) decreases as the void size increase, being smaller than 100^o in all cases. Thus one may infer that in the framework of the R&B model the voids have to be considered to be strong obstacles, i.e. the first equation in Eq. 2 is relevant for the critical stress calculations.

A surprising result of the present work is that the dislocation climbs when cutting through the void, if the void size is sufficiently large. This can be seen in Fig. 6 where the configuration of the dislocation after leaving the void, projected on the [111] plane, are presented. For convenience, the configurations of VOID_II and VOID_III are presented by shifting them on 1.5 and 3.0 periods along the $[10\bar{1}]$ direction, respectively. As can be seen from Fig. 6 in the case of VOID-I the dislocation keeps the initial straight configuration. It is interesting to note that when the dislocation enters the larger voids, a double jog

is first formed, with a separation between the jogs about equal to the void diameter.

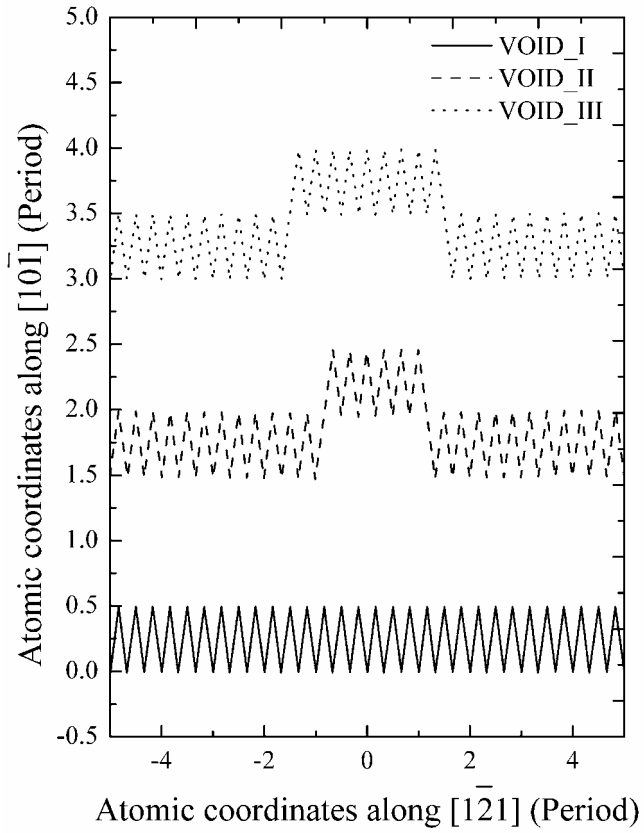

Figure 6 : Projection of the dislocation on [111] plane after the dislocation braking free of the voids. The projections for the VOID-II and VOID-III are presented by shifting them on 1.5 and 3.0 periods along $[10\bar{1}]$ direction, respectively. Note that in the cases of the VOID-II and VOID-III the dislocation climbs on a half of the unit in positive $[10\bar{1}]$ direction forming the two-unit jogs separated by a distance about the void diameter.

4.1 Core radius

Within the continuum isotropic elasticity theory, the strain energy of a dislocation in an isotropic cubic crystal is a linear function of $\ln(R)$, where R is the outer radius of a cylinder containing the dislocation core at its center. The strain energy may be divided into two parts, the core energy E_c stored inside the core area of a radius r_c, and the elastic strain energy stored outside the core. Then the total strain energy of the edge dislocation E can be written as

$$E = E_c + \Lambda \ln\left(\frac{R}{r_c}\right), \qquad \Lambda = \frac{\mu b^2}{4\pi(1-\nu)}, \tag{3}$$

where ν is the Poisson ratio. We can estimate the core radius, by comparing equation (3) with the total strain energy calculated from the atomistic simulations. Plotting E as a function of $\ln(R/b)$ in Fig. 7, a straight line is obtained when $R > 4.85b$, a value which can be estimated as the magnitude of the core radius. The corresponding core energy E_c, and parameter Λ are 16.6 eV/nm and 8.2 eV/nm, respectively. The value of Λ is equal to that calculate from the elastic moduli (see Eq. 3). We note the arbitrariness in the estimation of the core radius because the exact point at which the curve in Figure 7 becomes linear is not very well defined.

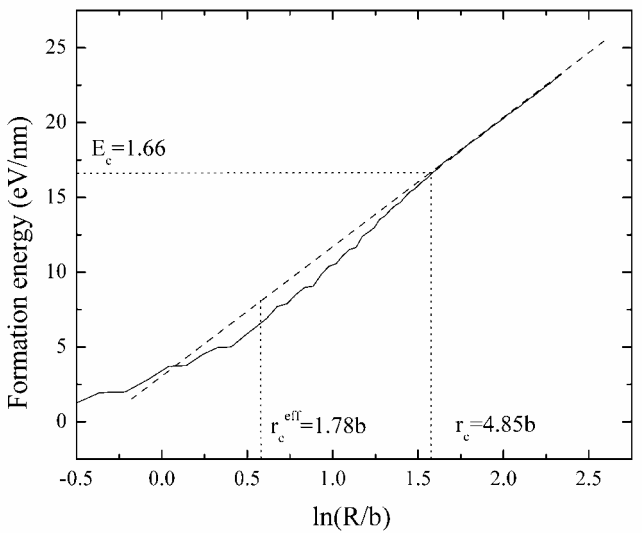

Figure 7 : Formation energy of $(a/2)\langle 111\rangle$ edge dislocation vs $\ln(R/b)$ obtained in the present calculations. The fitted calculation results above $\ln(R/b)$ =1.55 are shown as a dashed straight line.

4.2 Comparison with R&B model

The yield stress as a function of void radius between $1.75a$ and $4.0a$ has been calculated. The strengthening effect of the voids is found to be rather high, and increases rapidly with increasing void sizes. The core radius of the dislocation is found ($r_c = 4.85b$) to be larger that the radius of the largest void ($r^{max} = 4a \approx 4.62b$). It follows from the R&B model (Eq. 2) that the yield

stress due to the voids presently considered is zero. The large discrepancy between the atomistic and the continuum results is clear from Fig. 8, where the atomistic results (filled squares) are presented in comparison with predictions from the R&B model (dashed line) plotted as a function of the void radius. The latter is obtained using the first equation in Eq. 2, assuming the void spacing to be equal to the length of the simulation cell between the periodic boundaries, that is L =45.2b. The magnitude of the cut-off radius in the calculations is taken to be R = $10^6 r_c$, i.e., $\sim$2.5mm. From this comparison, one may tend to conclude that the R&B model is not suitable for describing the strengthening effects of small voids.

However, as can be seen from Fig. 8, the void-size dependence of the yield stress from both models is similar. Indeed, very good agreement between the simulations results and the predictions of the R&B model can be obtained if an effective dislocation core radius is used: $r_c^{eff} = 1.78b$ (solid line in Fig. 8). Other than the arbitrary nature of r_c, this agreement may also be understood, as reflecting the difference between the core radii under static and dynamical conditions.

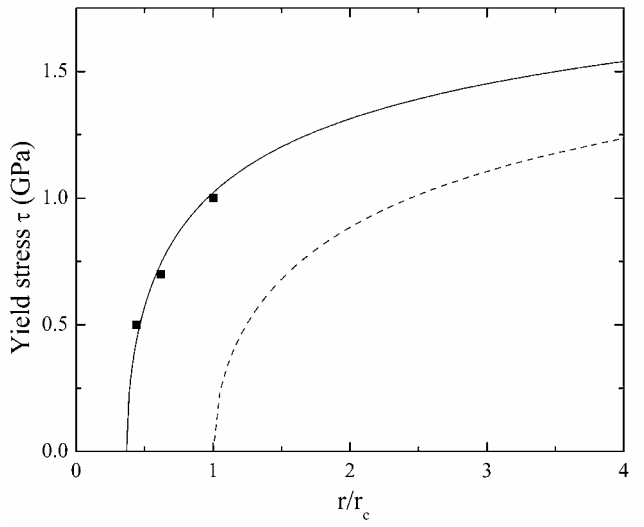

Figure 8 : Yield stress τ as a function of void radius as calculated in the present simulations and by using the first equation in Eq. 2. The points marked by the filled squares correspond to the yield stress calculated in present simulations. The dashed and solid lines correspond to the core radius of 4.85b and 1.78b, respectively.

5 Summary

For atomistic simulations involving moving dislocations, e.g., the bow-out of a dislocation under an external applied stress against a field of defects, image forces due to the necessary imposition of boundary conditions on a finite simulation cell, may produce artifacts and adversely affect the accuracy of the results. Despite the common use of such boundary conditions in many simulations to-date, there is an obvious need for a method that may alleviate this problem. The present work aims to contribute to this effort.

In the present work, the image forces due to the fixed boundaries is relaxed periodically, using the 3D GF, to allow the continuation of the dislocation motion and various reactions to take place. Our basic assumption is that a single GF relaxation is able to remove the built-up image forces due to the fixed boundaries. We test this assumption in the case of the glide of an edge dislocation under a shear stress much large than the Peierls stress.

The present method is applied to study the reaction between an edge dislocation in tungsten and an obstacle in the form of a void. Detail information on the reaction at the atomistic level is obtained, together with all the necessary parameters describing the void strengthening effect. The yield stress as a function of void size obtained in this work is not in agreement with that predicted by the continuum model, if the dislocation core radius is calculated on a basis of the MD static strain energy calculations (4.85b). However, the simulation results are in excellent agreement with the model if a smaller effective radius can be sued (1.78b). It is interesting to note that the dislocation is found to climb during its motion through a void, if the void is sufficiently large.

Acknowledgement: The work described in this paper was substantially supported by a central research grant from the Hong Kong PolyU (G-V942), partially by grants from the Research Grants Council of the Hong Kong Special Administrative Region (PolyU 5167/01E and PolyU 5173/01E).

References

Ackland, G. J.; Thetford, R. (1987): An improved n-body semiempirical model for body-centered cubic transition-metals. *Phil. Mag. A*, vol. 56, pp. 15—30

Basinski, Z. S.; Duesbery, M. S.; Taylor, R. (1972):

Interatomic Potentials and Simulation of Lattice Defects, Plenum Press, New York, pp. 537—546.

Chang, J. P.; Bulatov V. V.; Yip, S. (1999): Molecular dynamics study of edge dislocation motion in a bcc metal. *J. Comput. Aided Mater. Des.*, vol.6, pp. 165—173.

Daw, M. S.; Baskes, M. I.; Wolfer, W. G. (1986): *Modelling Environmental Effects on Crack Growth*, the Metallurgical Society, Warrendale, PA, pp. 99—121.

Daw, M. S.; Foiles, S. M.; Baskes, M. I. (1993): The embedded-atom method-a review of theory and applications. *Mater. Sci. Rep.*, vol. 9, pp. 251—310.

Diaz de la Rubia, T.; Zbib, H. M.; Khraishi, T. A.; Wirth, B. D.; Victoria, M.; Caturia, M. J. (2000): Multiscale modelling of plastic flow localization in irradiated materials. *Nature*, vol. 406, pp. 871—874.

Finnis, M. W.; Sinclair, J. E. (1984): A simple empirical n-body potential for transition-matter structure defects and mechanical properties. *Phil. Mag. A*, vol. 50 pp. 45—55

Gehlen, P.C.; Rosenfield, A. R.; Hahn, G. T. (1968): Structure of the <100> edge dislocation in iron. *J. Appl. Phys.*, vol. 39, pp. 5246—5254.

Ghoniem, N. M.; Cho, K. (2002): The Emerging Role of Multiscale Modeling in Nano- and Micro-mechanics of Materials. *CMES: Computer Modeling in Engineering & Sciences*, Vol. 3, No. 2, pp. 147-174.

Golubov, S. I.; Liu, X. L.; Huang, H.; Woo, C. H. (2001): GFCUBHEX: Program to calculate elastic Green's functions and displacement fields for applications in atomistic simulations of defects in cubic and HCP crystals. *Compu. Phys. Comm.*, vol. 137, pp. 312—324.

Granzer, F.; Wagner, G.; Eisenblatter, J. (1968): Atomic calculation of the core-structure, core-energy and Peierls-stress of an edge dislocation in NaCl. *Phys. Stat. Sol.*, vol. 30, pp. 587—600.

Hirth, J. P.; Lothe, J. (1973): Anisotropic elastic solutions for line defects in high-symmetry case. *J. Appl. Phys.*, vol. 44, pp. 1029—1032.

Hoagland, R. G.; Hirth, J. P.; Gehlen, P. C. (1976): Atomic simulation of dislocation core structure and Peierls stress in alkali-halide. *Phil. Mag.*, vol. 34, pp. 413—439.

Hull, D.; Bacon, D. J. (2001): *Introduction to Dislocations*, Fourth Edition, Butterworth-Heinemann, Oxford, pp. 79—81.

Liu, W. C.; Shi, S. Q.; Woo, C. H.; Huang, H. (2002): Dislocation Nucleation and Propagation During Thin Film Deposition Under Tension. *CMES: Computer Modeling in Engineering & Sciences*, Vol. 3, No. 2, pp. 213-218.

Liu, X. L.; Golubov, S. I.; Huang, H.; Woo, C. H. (2004): Glide of Edge Dislocations in Tungsten and Molybdenum. *Mater. Sci. Eng. A*, vol. 365, pp. 96-100.

Moncevicz, A.; Clapp, P. C.; Rifkin, J. A. (1990): Dislocation mobilities in NiAl from molecular dynamics simulations. *Defects in Materials Symposium*, Boston, MA, MRS, Pittsburgh, PA, pp. 213—218.

Ohsawa, K; Kuramoto, E. (1999): Flexible boundary condition for a moving dislocation. *J. Appl. Phys.*, vol. 86, pp. 179—185.

Olmsted, D. L.; Hardikar, K. Y.; Phillips, R. (2001): Lattice resistance and Peierls stress in finite size atomistic dislocation simulations. *Modelling Simul. Mater. Sci. Eng.*, vol. 9, pp. 215—247.

Perrin, R. (1974): Computer simulation of dislocations. *J. Phys. Paris, Collog.*, vol. 35, pp. C7/103—111.

Puls, M. P.; Norgett, M. J. (1976): Atomistic calculation of core structure and Peierls energy of an (a/2) [111] edge dislocation in MgO. *J. Appl. Phys.*, vol. 47, pp. 466—477.

Puls, M. P.; Woo, C. H. (1975): *Atomic Energy of Canada Limited Report* AECL-238.

Rao, S.; Hernandez, C.; Simmons, J. P.; Parthasarathy, T. A.; Woodward, C. (1998): Green's function boundary conditions in two-dimensional and three-dimensional atomistic simulations of dislocations. *Phil. Mag. A*, vol. 77, pp. 231—256.

Rodney, D.; Martin, G. (1999): Dislocation pinning by small interstitial loops: A molecular dynamics study. *Phys. Rev. Lett.*, vol. 82, pp. 3272—3275.

Rodney, D.; Martin, G. (2000): Dislocation pinning by glissile interstitial loops in a nickel crystal: A molecular-dynamics study. *Phys. Rev. B*, vol. 61, pp. 8714—8725.

Russell, K. C.; Brown, L. M. (1972): Dispersion strengthening model based on differing elastic-moduli applied to iron-copper system. *Acta. Metall.*, vol. 20, pp. 969—974.

Sinclair, J. E.; Gehlen, P. C.; Hoagland, R. G.; Hirth, J. P. (1978): Flexible boundary-conditions and nonlinear geometric effects in atomic dislocation modeling. *J. Appl. Phys.*, vol. 49, pp. 3890—3897.

Srivastava, D.; Atluri, S. N. (2002): Computational Nanotechnology: A Current Perspective. *CMES: Computer Modeling in Engineering & Sciences*, Vol. 3, No. 5, pp. 531-538.

Vitek, V. (1974): Theory of core structure of dislocation in body-centered cubic metals. *Cryst. Lattice Defects*, vol. 5, pp. 1—34.

Woo, C. H.; Puls, M. P. (1976): Improved method of calculating lattice friction stress using an atomistic model. *J. Phys. C: Solid State Physics*, vol. 9, pp. L27—L31.

Woo, C. H.; Puls, M. P. (1977): Atomistic breathing shell-model calculations of dislocation core configurations in ionic-crystals. *Phil. Mag.*, vol. 35, pp. 727—756.

Xu, W; Moriarty, J. A. (1996): Atomistic simulation of ideal shear strength, point defects, and screw dislocations in bcc transition metals: Mo as a prototype. *Phys. Rev. B*, vol. 54, pp. 6941—6951.